Analysis of Partial Discharges in Oil-Impregnated Transformer Paper Insulation and PET-G Insulation

Sayed Mohammad Kameli, *Student Member, IEEE*, Abdelaziz Abuelrub, *Student Member, IEEE*, Mohammad Al-Shaikh Saleh, *Student Member, IEEE*, Shady S. Refaat, *Senior Member, IEEE*, Ali Ghrayeb, *Fellow, IEEE*, Haitham Abu-Rub, *Fellow, IEEE*, and Marek Olesz

Abstract Partial discharge (PD) is a widespread phenomenon instigated in power transformer (PT) insulation systems. PDs are triggered by voids that vary in size and position within the PT insulation. The electrical characteristics of those damaging, PD-causing cavities must be well understood, to accelerate the development of advanced PD detection techniques. Thus, the impact of varying the radius and position of spherical air voids on the characteristics of PDs in PTs is examined using a 3D finite element analysis (FEA) model designed in COMSOL Multiphysics. The spherical voids are positioned between two windings of a 512 kV, three-phase (3ϕ) PT. The peak electric field (EF) and aggregate energy in the FEA model are used in conjunction with laboratory measurements of the apparent discharge magnitude, for detailed analysis of Polyethylene Terephthalate Glycol (PET-G) based cylindrical voids with different heights. Simulations demonstrate that the inception of PD activity in the PT model occurs for spherical voids with a radius exceeding 1 mm. Furthermore, the most severe PDs occur within the press-board insulation, adjacent to the uppermost part of the innermost windings. Experiments demonstrate that a significant increase in PD activity was observed for PET-G based cylindrical voids with heights exceeding 1 mm.

***Index Terms*—Dielectric breakdown, high-voltage techniques, insulation, partial discharges, power transformer**

I. INTRODUCTION

A. Background and Motivation

FAILURES of power transformer (PT) insulation may occur due to faults and defects in the PT, such as partial discharges (PDs), oxidation deposits, corrosion deposits, starting faults, and arcing faults, etc. [1]. PDs are common faults present in PTs and are a sign of insulation degradation [2]. PDs occur in insulating materials such as PT oil and pressboard insulation [3]. A survey of 972 PTs showed that out of all faulty PTs, 21% were diagnosed with PD activities [1]. Predicting faults is imperative for electric utilities since it helps extend their assets' operational lifetime. Moreover, the global market for asset condition monitoring is projected to grow to $5.2 billion by 2029 [4], hence, employing PD detection is key to ensuring reliable condition monitoring [5], avoiding unexpected shutdowns [6], and saving replacement and maintenance costs.

PD activity is initiated by the presence of air voids in PT oil-impregnated paper insulation. PD activity is associated with key characteristics such as discharge pulses, ultrasonic emissions, radio frequency emissions, inception voltage, progressive insulation degradation, and energy dissipation [7] – [11]. In [12], the authors investigated PT insulation in the presence of PDs by analyzing the breakdown characteristics of eco-friendly oil. In [13], the authors investigated the fiber Bragg grating sensors' application for PD monitoring in an oil-filled power transformer, discussing the advantages and disadvantages of the different methods of PD detection. In [14], the authors investigated the effect of adding inter-harmonic components to the fundamental frequency, for the detection and analysis of PDs. In [15] – [17], the authors developed antenna sensors, notably, the Hilbert fractal antenna and wideband antenna arrays for PD detection and localization. In [18], the author investigated the impact of heat-induced aging on oil-impregnated PT paper until breakdown, while concurrently analyzing the PD characteristics. The findings indicate that as the oil-impregnated paper undergoes thermal aging, both the quantity and intensity of PD events increase. Dielectric spectroscopy was conducted on the samples prior to and following PD aging, and the outcomes were employed to elucidate the evolution of PD behavior over time [18].

In [19], the author sought to correlate the PD and streamer features in three PT fluids subjected to AC voltage stress. The associations between PD and streamer attributes demonstrated that identical apparent charge values might signify distinct degrees of streamer progression within the insulation material, contingent on the consistency of the electric field (EF). This suggests that the interpretation of PD measurement

"This publication was made possible by NPRP grant [13S-0116-200085] from the Qatar National Research Fund (a member of Qatar Foundation). The statements made herein are solely the responsibility of the authors." *(Corresponding author: Sayed Mohammad Kameli)*.

Sayed Mohammad Kameli and Abdelaziz Abuelrub are with the Electrical and Computer Engineering department in Texas A&M University at Qatar, Doha, Qatar (e-mail: sayed.kameli@qatar.tamu.edu; a.abu_el_rub@qatar.tamu.edu).

Mohammad AlShaikh Saleh is with the Department of Electrical and Computer Engineering in Texas A&M University, College Station, TX 77843 USA (e-mail: mohammad.saleh@tamu.edu).

Shady S. Refaat is with the School of Physics, Engineering, and Computer Science, Department of Engineering, at the University of Hertfordshire (e-mail: s.khalil3@herts.ac.uk).

Ali Ghrayeb and Haitham Abu-Rub are with the Electrical and Computer Engineering Program in College of Science and Engineering, Hamad Bin Khalifa University, Qatar Foundation, Doha, Qatar (e-mail: aghrayeb@hbku.edu.qa; haburub@hbku.edu.qa).

Marek Olesz is with the Department of Electrical Power Engineering, Gdańsk University of Technology, 80-233 Gdańsk, Poland (e-mail: marek.olesz@pg.edu.pl).

Color versions of one or more of the figures in this article are available online at http://ieeexplore.ieee.org

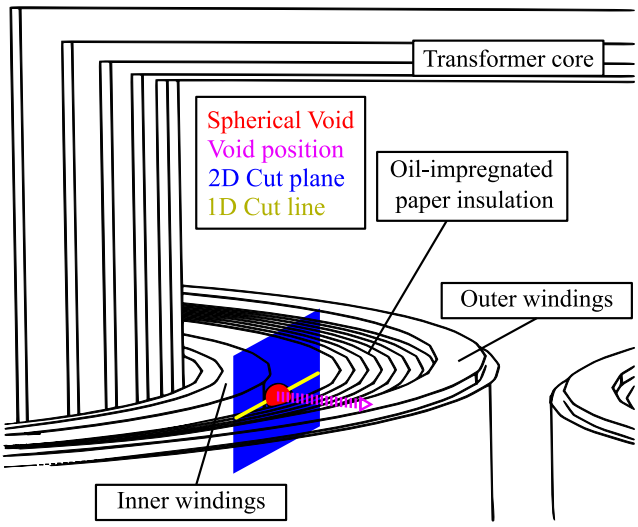

Fig. 1. Wireframe view of the PT FEA model and the spherical air void geometry.

outcomes should consider both the EF uniformity (PD location) and the type of liquid.

There is significant difficulty in reproducing the exact conditions initiating PD activity. It is therefore imperative to study the EF characteristics of PD inception instigated by voids in PT insulation using FEA and merging it with other measured attributes. The benefit of the FEA simulation of PD-causing voids is demonstrated in its ability to model the phenomenon while providing the freedom to evaluate physical quantities that could not be measured. This enhances the understanding of how voids influence various physical quantities of interest. The advantage of using EF in PD assessment is the availability of a known benchmark to compare against, the dielectric breakdown strength of air and the insulation itself. This nullifies the stochastic nature of PDs, as there is always uncertainty in assessing an asset's condition using alternative methods, such as ultrasonic acoustic emissions. This concept was previously used for high voltage (HV) XLPE cables in [20] – [22], where the authors investigated the relation between different void sizes, void positions, and PD activity. It was found that the EF distribution was an effective measure of an asset's condition, and the void position created a larger disturbance in the field distribution compared to the void size. The investigation does not include a detailed analysis of the total energy content within the air void, requiring an integration operator. Moreover, the fields in the PT follow a different distribution, requiring a study utilizing a PT's geometry. The simulations presented in this work reveal the unique properties of air voids submerged in oil-impregnated PT paper. Moreover, several experiments have been conducted to quantify the detriment of PD activity on PET-G insulation. Therefore, this paper investigates the effect of a spherical shaped void position and size on PD inception in PT insulation and addresses the acquired mathematical models for key parameters while incorporating practical HV tests of cylindrical shaped voids in PET-G insulation.

B. Contributions

The proposed solution offers a comprehensive study of the EF, energy, and apparent discharge magnitude. Pattern analysis was performed on charge-voltage-phase (Q-V-ϕ) data, and extensive statistical analysis was performed for PD fingerprinting. Prior work was related to the frequency content of the collected signals, increasing the set of useful features for the classification of void size and PD intensity. Two-dimensional (2D) vector analysis and one-dimensional (1D) scalar analysis were performed on the EF distributions of the void, enhancing the feature set. The collection of attributes analyzed in this paper paves the way for a novel, comprehensive system for PD analysis.

TABLE I
POWER TRANSFORMER SPECIFICATIONS

Parameter	Symbol	Value	Unit
Core relative permeability	μ_{Fe}	1200	none
Oil relative permittivity	ϵ_{oil}	2.1	none
Al_2O_3 paper relative permittivity	ϵ_{paper}	3.5	none
Density of soft iron	D_{Fe}	7900	kg/m^3
Stacking factor	K_i	0.95	none
Window space factor	K_w	0.16	none
Primary voltage	V_p	512	kV
Secondary voltage	V_s	132	kV

The main contributions of this paper are as follows.

1) The relation amongst energy, apparent discharge magnitude, and EF as PD intensity and location varies is revealed, and its effect on PD inception in HV PT insulation and PET-G insulation is studied.
2) A three-dimensional (3D) finite element model for analyzing the physical characteristics of PDs in PTs is built, to overcome the difficulty of measuring the EF physically.
3) Pattern analysis on charge-voltage-phase signatures from PET-G insulation, coupled with Fourier and statistical analysis is performed, for improvements in PD fingerprinting.
4) 2D vector and 1D scalar fields are analyzed, to consider PD events in a non-uniform EF distribution inside the cavity.

C. Paper Outline

The paper is organized as follows. Section II provides the 3D finite element analysis (FEA) model of the PT, and the accompanying vector and scalar analysis of the defects. Section III reveals the relation amongst void energy, apparent discharge magnitude, and peak EF intensity as void size and location vary. Pattern analysis on Q-V-ϕ signatures is also coupled with Fourier and statistical analysis. Section IV concludes the paper.

II. POWER TRANSFORMER FINITE ELEMENT ANALYSIS MODEL, VECTOR, AND SCALAR ANALYSIS

In this section, the simulation procedure of a 3D PT FEA geometry is presented, and rated specifications, along with results of some spatial plots of key vector fields and scalar quantities involving the defect are analyzed in detail.

A. Three-Dimensional Power Transformer Finite Element Model

The spatial distribution of the EF describes the conditions

This article has been accepted for publication in IEEE Open Journal of Instrumentation and Measurement. This is the author's version which has not been fully edited and content may change prior to final publication. Citation information: DOI 10.1109/OJIM.2025.3555323

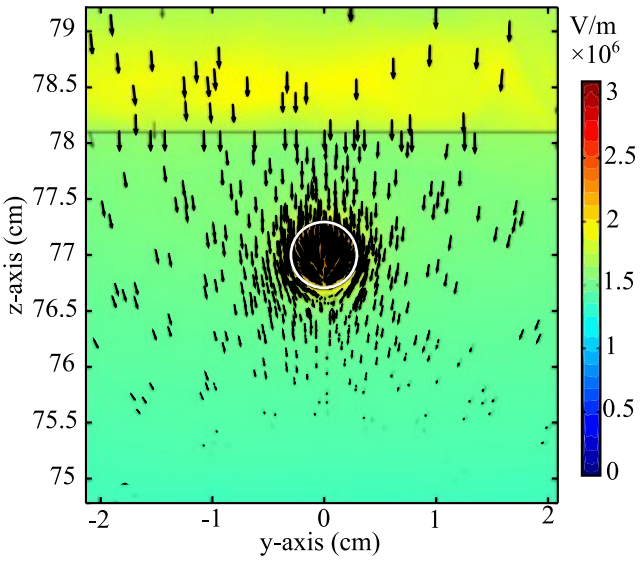

Fig. 2. Scalar and vector electric fields along a plane intersecting the air cavity. The electric field distribution is evaluated along the blue-colored 2D cut plane shown in Fig. 1.

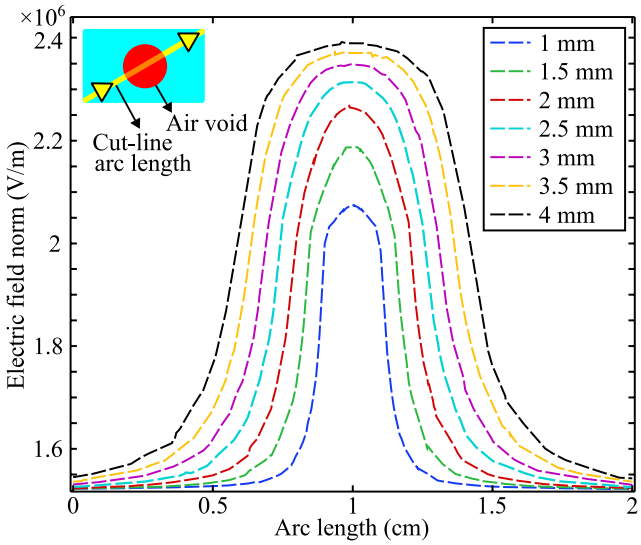

Fig. 3. Variation in EF norm along a cut line intersecting the spherical air cavity for different cavity radii. The EF norm is evaluated along the yellow colored 1D cut line shown in Fig. 1.

that occur during PD inception. The focus of the following discussion is the electrical aspect of the PT, providing details on quantities such as charge, EF, and energy. The faults in a three-phase (3ϕ) two-winding PT are modeled using FEA software. Table I shows the most prominent parameters defining the PT's geometric and electric properties. Fig. 1 illustrates a wireframe 3D view of the regions of a 3ϕ HV PT's geometry that is in close proximity to the spherical void studied in this paper. The PT components shown in Fig. 1 include the transformer core, outer windings, inner windings, and the oil-impregnated paper insulation. Each phase consists of a pair of concentric windings, an inner winding rated at 132 kV, and an outer winding rated at 512 kV. Fig. 1 also shows a close-up of the red spherical void embedded between the two windings of the leftmost phase of the PT. The distance between the center of the spherical void and the inner winding is 1.08 cm. When changing the void position, the void remains the same size but is shifted along the magenta trace. A custom mesh was used, with a maximum element size, minimum element size, maximum element growth rate, and curvature factor of 8.4 cm, 0.003 cm, 1.3 (unitless), and 0.2 (unitless), respectively. A suitable maximum mesh element size of 8.4 cm allows for a reasonable simulation time, while a minimum mesh element size of 0.003 cm ensures that the mesh fineness within the void's vicinity is sufficient to resolve the electric fields correctly. The maximum mesh element growth rate has been tuned to 1.3 to prevent large discrepancies between the volumes of adjacent tetrahedral mesh elements, and the curvature factor was tuned to 0.2 to prevent coils from rendering incorrectly during modeling.

B. Scalar and Vector Field Analysis of Air Voids in Oil-Impregnated Transformer Paper

To evaluate the damaging effect of air pockets on a PT insulation's field distribution, 2D plots of the EF are obtained, revealing regions of severe electrical stress within the spherical void. All the quantities shown in the 2D plots are evaluated along the blue surface of Fig. 1. A plot of the EF vector field within the spherical void's vicinity is shown in Fig. 2. The flux density is consistent for the majority of the regions surrounding the spherical void, with a noticeable decrease in the flux density below the void, due to the attenuation of the field strength. Peak flux density occurs within the void, a hotspot for PD events. This is due to the lower permittivity of the void, causing higher local and inhomogeneous field line concentrations, exceeding the dielectric strength of the surrounding material, leading to insulation degradation and breakdown. To identify the EF intensity and direction, a scalar-vector plot group is displayed in Fig. 2. It is observed that some fields outside the spherical void have the propensity to assume a direction tangent to the void's contour, and there is an increasing concentration of field vectors within the void relative to its surroundings, confirming the large electrical stresses present from voids. The heatmap shows a nonuniform orientation of electric field vectors and high stresses in the regions of Fig. 2 within, above, and below the spherical air void (outlined in white). The vector field and heatmap results in Fig. 2 are based on an evaluation of the FEA model along the blue cut plane, as shown in Fig. 1.

C. Effect of Cavity Size on the Electric Field Distribution

To illustrate the effect of cavity size on the EF distribution along one dimension, the EF norm was obtained for a family of cutline plots, each representing a certain spherical void radius, as seen in Fig. 3. The cutline is defined as the yellow curve intersecting the red void in Fig. 1. Seven spherical voids, with radii {1 mm, 1.5 mm, 2 mm, 2.5 mm, 3 mm, 3.5 mm, 4 mm} are investigated, revealing relations not observed in the 2D heatmaps. This range of void radii was selected since it was found that PD activity is initiated for spherical voids with a radius exceeding 1 mm. The EF norm within all voids is larger than the surrounding paper insulation, and an increase in the central EF norm at an arc length of 1 cm is observed as the spherical void radius increases. The arclength is defined as the Euclidean distance between a point that lies on the cutline and the endpoint of the cutline. This is a side effect of the spike in electrical field value

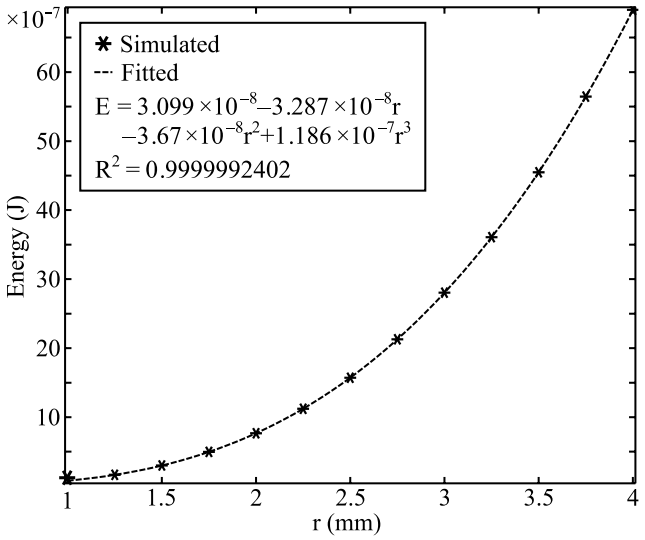

Fig. 4. Aggregate electrical energy in spherical air void vs radii.

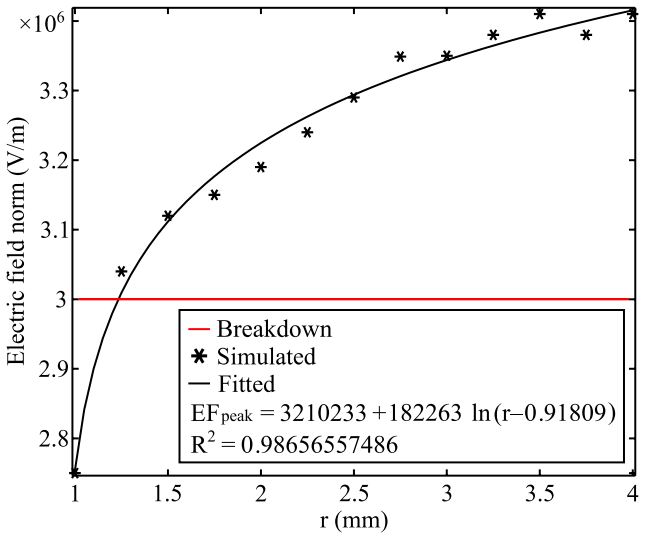

Fig. 5. Peak EF norm in spherical air void vs void radii.

caused by the surface area of the larger void. The 4 mm spherical void exhibits the highest EF intensity, with a peak EF norm of 2.4 MV/m, less than the 3 MV/m threshold required for the inception of PD activity [25].

III. Partial Discharge Pattern Analysis Based on Void Size and Position

To facilitate a more accurate condition monitoring system, the relation among void energy, apparent discharge magnitude, and peak EF intensity as a function of void size and location is derived from experiments and FEA modeling. Pattern analysis on Q-V-ϕ signatures is coupled with Fourier and statistical methods for a more robust feature set.

A. Modelling the Effect of Void Size on Partial Discharge Activities

Air voids are a source of concern in PTs, as they seed PD activities. Voids of different sizes exist within the PT's insulation system, indicating various stages of deterioration. It is essential to have a reference on the level of EF inhomogeneity caused by voids of different sizes, to accurately benchmark the stages of insulation aging effectively. Fig. 4 shows the correlation between the electrical energy content of a spherical void and its radius, computed by performing a volumetric integral of the energy density within the spherical void, expressed as [26]

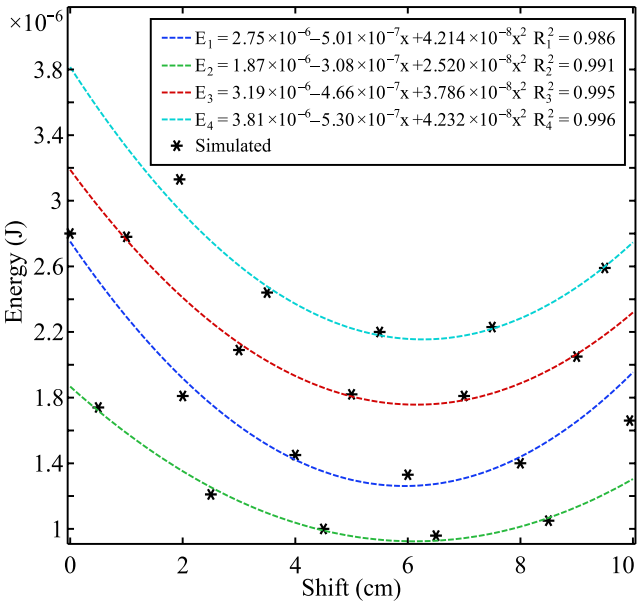

Fig. 6. Aggregate electrical energy in spherical void vs position.

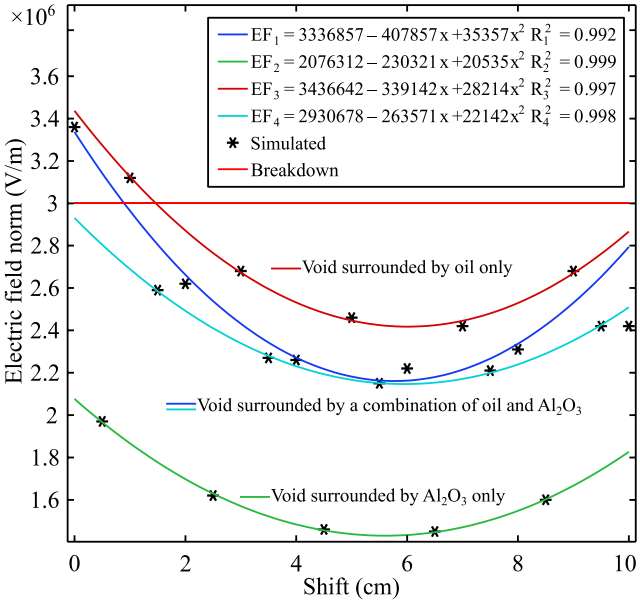

Fig. 7. Peak electric field norm in spherical air void vs position.

$$E = \iiint_{x\,y\,z} U(x,y,z)\,dxdydz\,, \tag{1}$$

where E is the total electrical energy content of the void in J, and U is the energy density in J/m^3, evaluated by solving for (2), the energy density at a certain point in space, where ε is the insulation material's permittivity, and E_f is the electric field.

$$U = \frac{1}{2}\varepsilon E_f^{\,2} \tag{2}$$

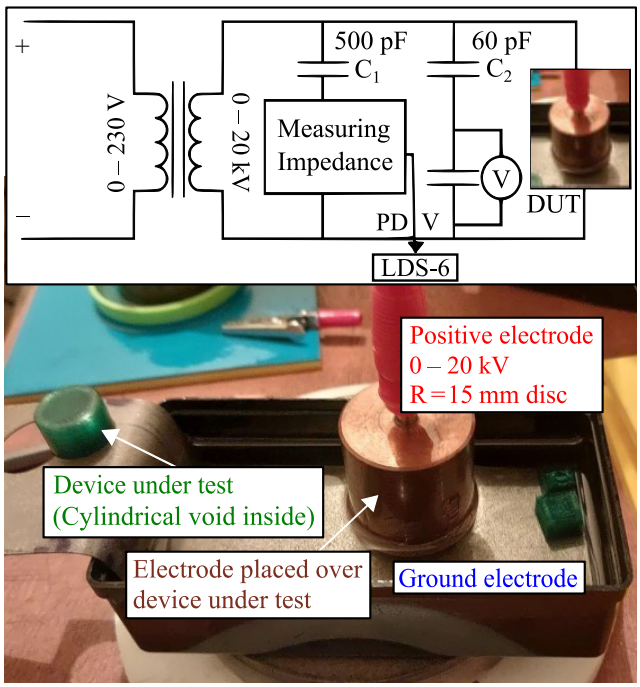

Fig. 8. High voltage setup and circuitry used for stressing the cylindrical air void.

It was determined that the equation of best fit was a cubic function, represented by the continuous curve of Fig. 4. The fitness of the obtained curves is based on the coefficient of determination, or R^2 metric, which is the square of the correlation coefficient [27].

The model fits well with the discrete simulated values, with an R^2 metric of 0.9999. The R^2 metric approaches unity due to the spherically symmetric energy distribution of all spherical voids, creating a direct relation with the cube of the radius. The peak EF norm refers to the highest magnitude of the EF stress within a void and is directly related to the stress experienced by the insulation material surrounding the void. It provides insights into the performance of insulation systems during high stress. Fig. 5 is a graph of the peak EF norm within the spherical voids as a function of their radii, generated by utilizing a feature in COMSOL Multiphysics known as the derived values feature. The derived values feature [28], allows for the evaluation of the maximum value of any dependent field quantity, such as the electric field norm (the electric field amplitude), within a subset of the three-dimensional space. In this case, the derived values feature in COMSOL is used to obtain the maximum electric field instigated in the voids. The maximum values of the electric field norm are directly obtained from the solution dataset, determining the severity of PD occurrence within the dielectric material. It is demonstrated that the rate of increase of the EF norm is always positive and is greater for smaller radii compared to larger radii. The logarithmic function fits very well, capturing both rates of change, as seen in Fig. 5. The R^2 value was found to be 0.9865 ± 1E-5. It can be deduced that PD activity is likely to ensue with spherical voids whose radii are larger than 1 mm, attributed to the increased quantity of electric field lines intersecting the void, and the curvature of the flux lines from the air-oil interface.

TABLE II
INCREASE IN PEAK APPARENT DISCHARGE MAGNITUDE FOR CYLINDRICAL VOIDS AT DIFFERENT HEIGHTS.

Height Increase	Positive Peak Apparent Discharge Magnitude (-)	Negative Peak Apparent Discharge Magnitude (-)
1 → 2 mm	8.18	6.23
2 → 3 mm	1.41	1.72
3 → 4 mm	1.93	1.92
4 → 5 mm	0.71	0.54
5 → 6 mm	4.40	6.01

TABLE III
STATISTICAL FINGERPRINTS OF THE CYLINDRICAL VOIDS AT DIFFERENT HEIGHTS.

Height	Variance (-)	Skewness (-)	Kurtosis (-)
1 mm	5618.565	0.067	27.060
2 mm	57889.974	−5.270	131.907
3 mm	79844.688	−1.689	150.155
4 mm	207651.468	0.336	720.150
5 mm	222316.451	−2.49	181.819
6 mm	5575909.86	−1.553	362.661

B. Modelling the Effect of Void Position on Partial Discharge Activities

As the insulation condition worsens, voids get larger due to increased gas buildup from the decomposition of transformer oil [29], further deteriorating the insulation's performance. It may also be the case that PD activity is noticed irregularly as a void migrates within the PT's tank to regions with high EFs. It is essential that the damaging effect of a void's position in a region of concern, such as between the windings of a transformer [5], is probed. Fig. 6 shows the total electrical energy within a spherical void (r = 1 mm) as a function of the void's position. The figure was generated by shifting the position of the spherical void along the magenta-colored trace of Fig. 1 and integrating the energy density within the void for each shift value. The spherical void is surrounded by a non-homogenous material, the oil-impregnated PT paper. This causes the void to undergo a cyclic behavior as its membrane is surrounded by materials of alternating permittivity. For every shift of 0.5 cm in the −x or +x direction, a changing percentage of the void's volume is surrounded by the PT paper insulation. For every 2 cm shift towards one of the windings, the spherical void ends up being surrounded by the same material composition, causing a regular pattern to form. The pattern was identified as a family of quadratic functions whose y-intercept was strongly influenced by the surrounding material. To visualize this pattern, the data points in Fig. 6 are partitioned into four categories, based on the material composition of the insulation adjacent to the corresponding air void's boundary. Each category is fit with a quadratic function, and each fit is labelled with a color corresponding to the insulation material surrounding the void. The exact composition of the surrounding material is discussed in the following text.

Fig. 7 is a plot of the peak EF norm in the spherical void for various void positions. The strong dependency of the peak EF norm on the surrounding material's composition is shown. The peak EF generally increases when the void is

This article has been accepted for publication in IEEE Open Journal of Instrumentation and Measurement. This is the author's version which has not been fully edited and content may change prior to final publication. Citation information: DOI 10.1109/OJIM.2025.3555323

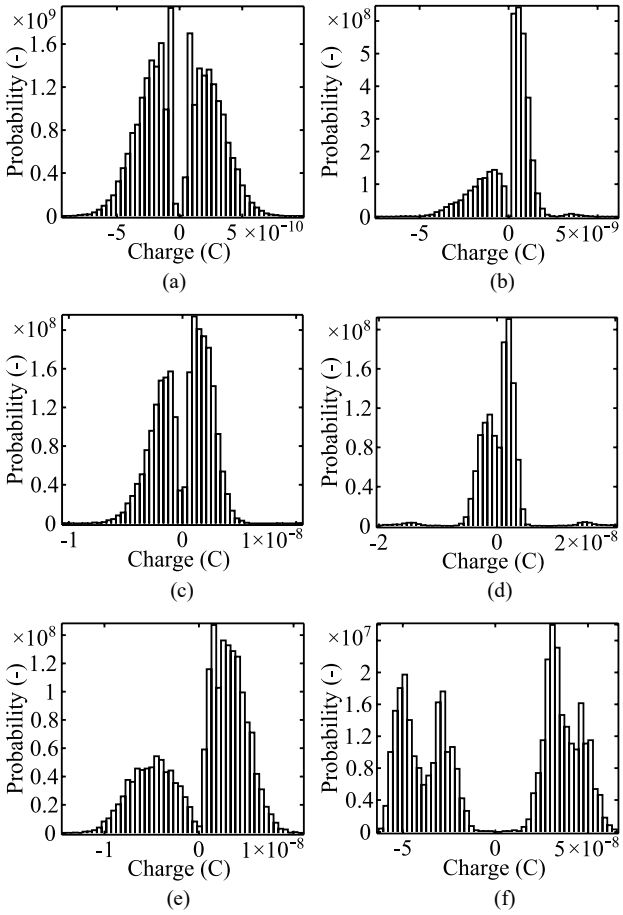

Fig. 9. Histogram of apparent discharge magnitudes for cylindrical voids with heights of (a) 1, (b) 2, (c) 3, (d) 4, (e) 5, and (f) 6 mm.

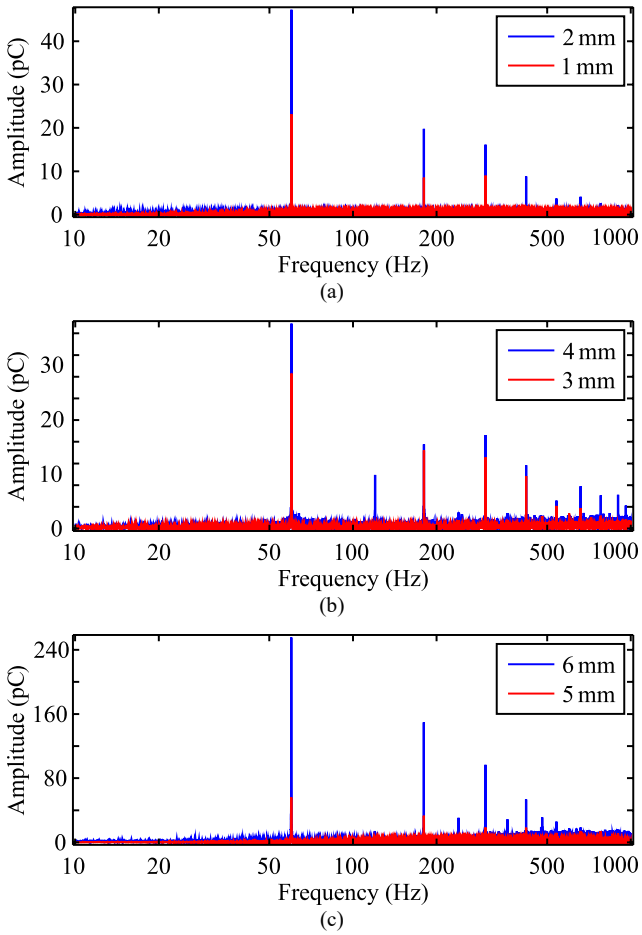

Fig. 10. Fourier Transform of the LDS-6 system's temporal discharge signals for cylindrical voids with heights of (a) 1 and 2 mm, (b) 3 and 4 mm, and (c) 5 and 6 mm.

fully submerged in the oil between the transformer paper layers, as indicated by the red trace of Fig. 7. On the other hand, the peak EF norm generally decreases as the void is positioned within the paper insulation layer, as indicated by the green trace of Fig. 7. This is a direct consequence of the lower relative permittivity of PT oil (2.1) when compared to the relative permittivity of PT paper insulation (3.5). The peak EF values between the paper insulation and oil, as shown by the indigo and cyan curves, have varying intensities, as seen in Fig. 7. The curves are best modeled by four quadratic functions. Moreover, it was observed that peak EFs occurred near the inner and outer windings of the PT, at shift values of 0 cm and 10 cm, respectively. This is attributed to the increase of flux lines cutting the spherical void's surface area when the void approaches the windings. Peak EF values of 3.37±0.1 MV/m were found near the innermost winding, sufficient to initiate PDs. This proves the importance of having flawless PT paper insulation adjacent to the transformer windings.

C. Fingerprinting Using Statistical, Spectral, and Charge-voltage-phase Signatures

To guarantee the prompt classification of air voids, fingerprinting techniques utilizing a diverse set of features must be used. The following will demonstrate the utilization of Q-V-ϕ patterns for fingerprinting. Cylindrical voids were created with a 3D printer using a Polyethylene Terephthalate Glycol (PET-G) filament. The experimental setup consists of a positive disc-shaped electrode with a radius of 15 mm and a flat ground electrode. A 20 kV RMS source was supplied at the positive electrode, 1 minute for each cylindrical void height. The cylindrical cavity diameter was set to 8 mm, and the cavity height was adjusted from 1 mm to 6 mm. The cylindrical cavities reside inside the green cylinders of Fig. 8. Cylinders were used, due to the difficulty in creating flawless spherical voids of sub-1 mm radius. 20 pC was used to calibrate the setup, using an LDC-5 calibrator producing a pulse train of charges. The external circuitry [30] powering the device under test (DUT) and cavity is shown. Time-domain discharge signals were collected using an LDS-6 PD measurement system.

Due to the unfavorable mechanical properties of transformer paper, it was realized that creating artificial voids that mimic voids found in aged oil-impregnated transformer paper was not suitable. Alternatively, 3D-printed PET-G based voids were utilized, ensuring results involving samples of the same size provided consistent degradation data. The relative permittivity of the PET-G inclusions used in the experimental validation falls within the 3 – 3.4 range, which is close to the power transformer paper insulation's permittivity of 3.5. To further improve the efficacy of the results and avoid the distortions found during fabricating voids using a 3D printer, cylindrical voids were used in place of spherical

This article has been accepted for publication in IEEE Open Journal of Instrumentation and Measurement. This is the author's version which has not been fully edited and content may change prior to final publication. Citation information: DOI 10.1109/OJIM.2025.3555323

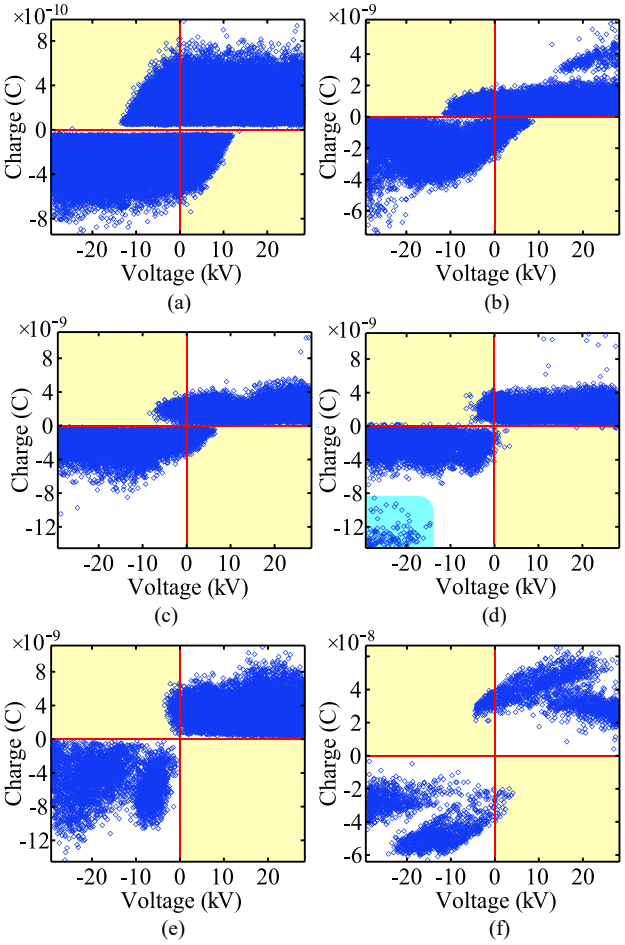

Fig. 11. Apparent discharge magnitude vs voltage scatter plots for cylindrical voids with heights of (a) 1, (b) 2, (c) 3, (d) 4, (e) 5, and (f) 6 mm.

voids. Since electric fields are strongly polarized along the z direction, scaling the height of the cylinders parallel to the field lines captures the main degradation mechanism found in the simulations, caused by strong z-direction polarization of the EF which is observed in Fig. 2. This simplifies the experimental setup by enabling the use of an anisotropically scaled cylindrical void rather than an isotropically scaled spherical void, bypassing fabrication issues that jeopardize the efficacy of the results. An anisotropically scaled cylindrical inclusion captures the trends observed in an isotopically scaled spherical inclusion effectively since the electric fields in both cases are predominantly polarized in the z-direction.

1) Fingerprinting Using Statistical Signatures

The peak apparent discharge magnitude for the sample with no void is very small, with a slight increase once a cylindrical void with a height of 1 mm is introduced. Results in Table II indicate that a substantial increase in observed discharge activity occurs as the cylindrical void height increases from 1 mm to 2 mm, with an increase in peak positive and negative apparent discharge magnitudes by 6.23 and 8.18 times, respectively, as shown in Table II. The abrupt increase in the peak apparent discharge magnitude presents a surge in PD activity, a strong indicator of exceeding the dielectric strength of the sample under test. Moreover, the increases in peak apparent discharge magnitudes as the cylindrical void height increases from 1 mm to 2 mm is higher than all subsequent increases in height.

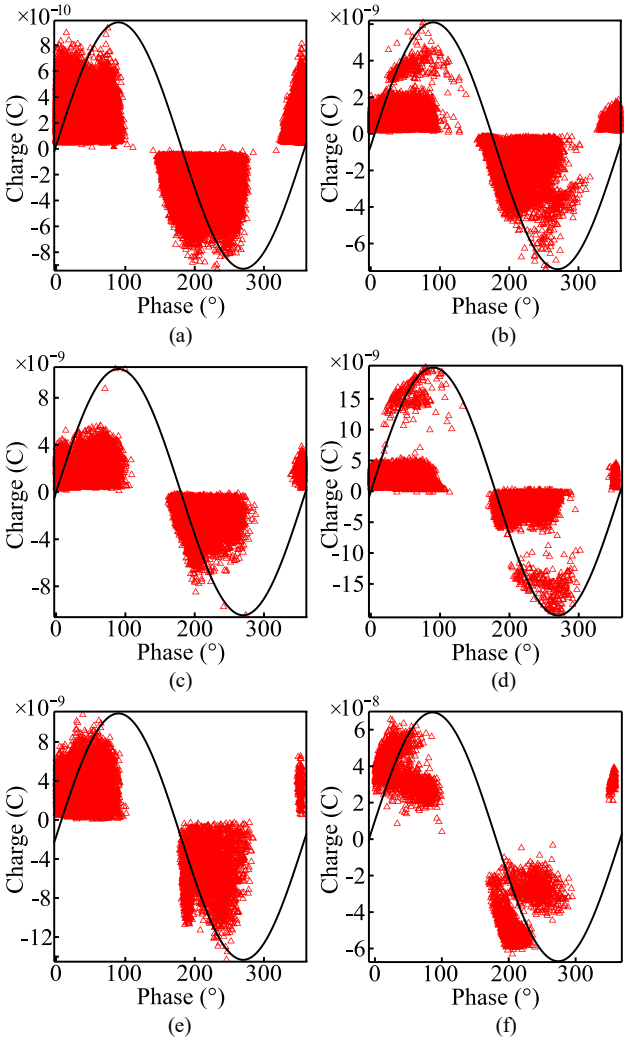

Fig. 12. Apparent discharge magnitude vs phase scatter plots for cylindrical voids with heights of (a) 1, (b) 2, (c) 3, (d) 4, (e) 5, and (f) 6 mm.

Fig. 9 shows histograms of PD levels in Coulombs for cylindrical voids of different heights, revealing the change in PD distribution as the insulation degrades. The discharge distribution in Fig. 9 (a) for the cylindrical void with a height of 1 mm is relatively symmetric, while a significant loss of symmetry is observed for the 2 mm cylindrical void in Fig. 9 (b), due to a substantial increase in PD activity. Some of the larger voids deviate more from the normal distribution by exhibiting varying levels of skewness, kurtosis, and variance, as listed in Table III. Asymmetry in the charge distributions is a consequence of the dissimilarity between the positive and negative half cycles. This dissimilarity stems from the higher mobility of electrons relative to holes, a result of the electron's lower mass. Moreover, the variance increases significantly as the cylindrical void's height increases, attributable to the increase in the concentration of high-magnitude PDs, as shown in Figs. 9 (e) and (f). The deviation in the discharge magnitudes from the origin, as shown in Fig. 9 (f), is a consequence of the increase in the concentration of high-magnitude PDs. The strongly skewed distributions in Fig. 9 are observed to be leaning toward positive charges, confirmed by the skewness values of the 2, 3, 5, and 6 mm cy-

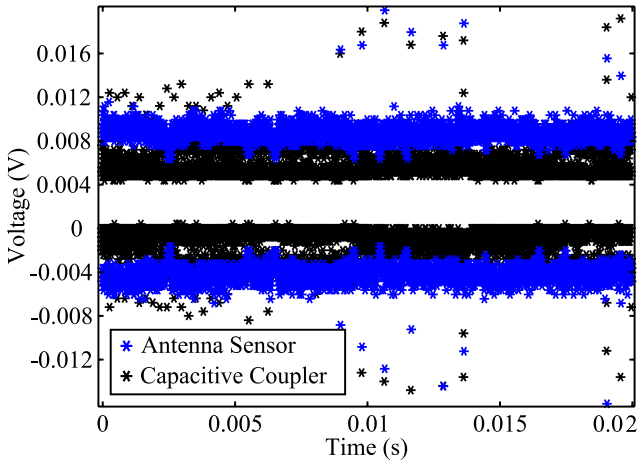

Fig. 13. PD signal received by an antenna vs a CC-TEV sensor for 1 power cycle.

lindrical voids found in Table III. The kurtosis values of Table III illustrate that the charge content of PDs is primarily populated in the tail regions of the distributions, as the central area is primarily populated by noise.

2) Fingerprinting Using Spectral Signatures

The frequency spectrum of a signal indicates important properties that cannot be resolved in the time domain. For instance, the energy content of the fundamental 60 Hz frequency component may be used for comparisons, or the ratio of two or more frequency components for different signals might reveal more information about the fault severity.

Fig. 10 shows the Fourier Transform (FT) [31] of signal $f(t)$, measured for each cylindrical void height. The spectral content of the signals is mainly harmonics of the fundamental frequency (60 Hz), with significant energy up to the 15th harmonic. As the cylindrically shaped void's height increases, the number of spectral lines that can be resolved from the noise floor generally increases, due to the increase in PD activity. Fig. 10 shows that the 1, 2, 3, 4, 5, and 6 mm cylindrical voids possess 3, 6, 8, 10, 4, and 10 spectral lines, respectively. The cylindrical void with a height of 5 mm seems to be the anomaly, since the number of spectral lines decreased, instead of increasing. This may be due to 3D printer fabrication errors, such as stringing, causing strings of PET-G filament to occupy the void, instead of air. Regardless, a consistent increase in the apparent discharge magnitude at the fundamental 60 Hz frequency is observed as the cylindrical void height increases, while a less direct correlation was observed for the harmonics. The increase in the amplitude at 60 Hz for larger voids is due to the increase in PD activity and the quantity of charge being transferred each cycle. It is concluded that an increase in the magnitude of the 60 Hz frequency component indicates advanced stages of PT insulation degradation better than the harmonics after the second order. This signifies that the 60 Hz frequency component can be used as a metric for insulation degradation and the level at which voids compromises the health of the insulation system.

3) Fingerprinting Using Charge-voltage-phase Signatures

Fig. 11 shows six scatter plots of the apparent discharge magnitude vs voltage for the cylindrical voids with heights of 1 mm – 6 mm. The four quadrants are separated using red lines, and regions of low PD activity are highlighted in yellow. The x-axis range is from −28.28 kV to 28.28 kV for all voids. Strong symmetry is observed in Fig. 11 (a), Fig. 11 (c), and Fig. 11 (f), while an increase in PD activity in the cyan region of Fig. 11 (d) is observed. In the yellow quadrants, a minority of negative PDs occur during the positive half cycle, and a minority of positive PDs occur during the negative half cycle, and PD charge polarity tends to obey the phase angle. The PDs occurring outside their half-cycle exhibit a hysteresis-like delay behavior as the charge polarity remains matching the previous half-cycle even during the initial stages of the current half-cycle. The proportion of PD activity in the shaded region relative to the unshaded region decreases as the cylindrical void's height increases. The distribution of PDs in the upper right quadrant is similar for all void heights, but the PDs for the 6 mm cylindrical void in Fig. 11 (f) are more elevated from the horizontal red line. All the aforementioned details form the basis for the Q-V PD fingerprint discussed previously.

The Phase Resolved Partial Discharge (PRPD) method is a well-renowned method that reveals the electrical phase angles that PDs most frequently occur in, and the apparent discharge magnitudes of the PD activity at that phase angle [21] – [23]. The analysis of PD behavior within the PT insulation system, in light of the provided six PRPD plots, is shown in Fig. 12, revealing compelling insights into the insulation condition and the relationship between PD and cylindrical void height ranging from 1 mm to 6 mm. The PRPD patterns observed in Fig. 12, were obtained by applying a source voltage of 20 kV RMS on the PET-G samples for approximately 3600 cycles. These PRPD patterns not only highlight the concentration of internal discharges at specific phase angle ranges, such as 0 to 100 degrees, and 150 to 270 degrees, but also introduce a critical dimension to the analysis, as they reveal the increase in occurrence and intensity of PDs for all phase angles. The occurrence and severity of PD activity are the ideal indicators of insulation degradation.

The observation of void size-dependent trends within these PRPD patterns is particularly noteworthy. As the height of the cylindrical void increases, the behavior and distribution of PDs evolves. Smaller cylindrical voids (1 to 2 mm height) may exhibit a scattering of discharges across various phase angles, suggesting localized, but less pronounced, electrical stress concentrations. In contrast, larger cylindrical voids (3 to 6 mm height) tend to manifest as more concentrated clusters of discharges within narrower phase angle ranges, indicating heightened EF stress at specific points within the PT insulation. These patterns imply that void size plays a crucial role in shaping PD behavior, with larger voids causing more severe insulation defects and discharges.

To translate these findings into actionable insights, simulations were conducted to correlate cylindrical void sizes with specific PD behavior and defect locations, which is among the main contributions of this paper. By analyzing the Q-V-ϕ data comprehensively, PT operators can make informed decisions about maintenance scheduling and repair priorities based on the void/defect severity within the PT insulation. Continuous monitoring and data analysis remain es-

sential for tracking changes in Q-V-ϕ data over time and ensuring the long-term reliability and safety of electrical systems. This holistic approach, incorporating both phase analysis and void size considerations through experimentation and FEA simulations, underscores the significance of detailed Q-V-ϕ analysis in managing and mitigating potential PT insulation issues. Consequently, this compendious study portrays the potential of the proposed simulation model to become an accurate digital twin model for evaluating different defect types and severities within the PT insulation system, driving down maintenance and testing costs, providing a better understanding of the innate insulation behavior in the presence of defects, and enhancing the reliability and stability of the power equipment present in the grid.

4) Comparison Between LDS-6, Antenna, and CC-TEV Measurements for Void Size Fingerprinting

A comparison between the charge-based LDS-6 measurement method utilized for Figs. 11 and 12 and two popular PD measurement methods, the ultrahigh-frequency antenna-based method, and the transient earth voltage capacitive coupler (CC-TEV) method is performed. This probes the effectiveness of the aforementioned methods in linking void size and PD activity. Fig. 13 compares the PD signal captured using an antenna [32] to a CC-TEV sensor over one cycle, measured using an oscilloscope in peak-to-peak mode. It can be observed that both the antenna and CC-TEV sensors exhibit similar fingerprints over the power cycle, both successfully detecting PDs with similar magnitudes. However, the noise level for the antenna is higher than the CC-TEV, due to interference from external noise sources. Moreover, the CC-TEV sensor detected more peaks than the antenna sensor, with a better signal to noise ratio. When comparing Figs. 11 and 12 (in coulombs) to the CC-TEV results from Fig. 13 (in volts), it is evident that the LDS-6 provides significantly more detailed discharge patterns. Although the antenna and CC-TEV are more convenient for use in the field, sensitive systems measuring the apparent discharge magnitude of PDs provide results more suitable for verifying simulations of the effect of void size on PD activity. Moreover, an increase in the peak EF of voids in simulations can be better associated with an increase in the apparent discharge magnitude due to an increase in void size.

IV. Conclusion

This study was performed to analyze the effect of different air-filled void sizes and positions on the characteristics of PDs in a 512 kV 3-phase PT. A 3D FEA model was proposed and built in COMSOL Multiphysics to study the behavior of spherical PD-producing voids in detail. The distortion in the scalar and vector fields in areas adjacent to the void were examined, and the phenomenon behind such distortions were inspected. The study focused on critical parameters such as the peak EF and aggregate energy of spherical PD-causing voids of various radii and positions in conjunction with laboratory measurements of PD inception voltage and peak apparent discharge magnitude of cylindrical PD-causing voids of different heights, for detailed time domain and frequency domain analysis. Mathematical models characterizing the peak EF and aggregate electrical energy were derived from the FEA model. The analysis of the peak apparent discharge magnitude involved utilizing Q-V-ϕ fingerprinting, to obtain better correlations between the simulated quantities and measured quantities. To further enhance the analysis presented in this work, statistical studies were performed to relate the stochastic nature of experimentally obtained PD data to simulated data. The following summarizes the main findings and presents recommendations for future work.

- Results illustrated that the inception of PD activity occurs for cylindrical voids with a height exceeding 1 mm and spherical voids with a radius exceeding 1 mm, indicating the damage of small air voids on surrounding insulation.
- It is essential that power transformer designers consider the threshold size of voids that lead to PDs in their designs.
- It is recommended that the temporal behavior of clusters of voids in close proximity are analyzed, as they can disrupt the uniformity of the EF in the transformer paper.
- It was also found that voids adjacent to the two windings of the PT were most susceptible to PDs. This suggests that the innermost and outermost transformer paper layers are subject to the greatest aging stresses.
- It is recommended that the effect of utilizing different types of insulation for the innermost and outermost transformer paper insulation layers are investigated. Insulation materials with high absorption capacity of transformer oil are an ideal solution for preventing voids.

There are no clinical implications of the work presented in this paper.

Acknowledgment

This publication was made possible by NPRP grant [NPRP13S-0116-200085] from the Qatar National Research Fund (a member of Qatar Foundation). The statements made herein are solely the responsibility of the authors.

References

[1] R. Jadim, M. Kans, J. Schulte, M. Alhattab, M. Alhendi, and A. Bushehry, “On approaching relevant cost-effective sustainable maintenance of mineral oil-filled electrical transformers,” *Energies*, vol. 14, no. 12, p. 3670, 2021.

[2] R. C. Kiiza, M. G. Niasar, R. Nikjoo, X. Wang and H. Edin, “Change in partial discharge activity as related to degradation level in oil-impregnated paper insulation: effect of high voltage impulses,” in *IEEE Transactions on Dielectrics and Electrical Insulation*, vol. 21, no. 3, pp. 1243-1250, June 2014, doi: 10.1109/TDEI.2014.6832271.

[3] S. Li, W. Si and Q. Li, “Partition and recognition of partial discharge development stages in oil-pressboard insulation with needle-plate electrodes under combined AC-DC voltage stress,” in *IEEE Transactions on Dielectrics and Electrical Insulation*, vol. 24, no. 3, pp. 1781-1793, June 2017, doi: 10.1109/TDEI.2017.006361.

[4] Machine Condition Monitoring Global Market Report 2022: Rising Focus on Reducing Human Intervention in Predictive Maintenance Presents Opportunities - ResearchAndMarkets.com

[5] S. M. Kameli, S. S. Refaat, A. Ghrayeb, H. Abu-Rub and J. Guziński, “Propagation Characteristics of Partial Discharges in an Oil-Filled Power Transformer,” *2023 IEEE 17th International Conference on Compatibility, Power Electronics and Power Engineering (CPE-POWERENG)*, Tallinn, Estonia, 2023, pp. 1-6, doi: 10.1109/CPE-POWERENG58103.2023.10227470.

[6] G. C. Stone, H. G. Sedding and M. J. Costello, “Application of partial discharge testing to motor and generator stator winding maintenance,” in *IEEE Transactions on Industry Applications*, vol. 32, no. 2, pp. 459-464, March-April 1996, doi: 10.1109/28.491498.

[7] A. Cavallini, C. G. A. Ramos, G. C. Montanari, J. Rubio-Serrano and J. A. Garcia-Souto, "Comparison of ultrasonic, electrical and UHF characteristics of partial discharge emission in oil/paper insulation systems," 2011 Annual Report Conference on Electrical Insulation and Dielectric Phenomena, Cancun, Mexico, 2011, pp. 440-443, doi: 10.1109/CEIDP.2011.6232689.

[8] R. Sangineni, T. Chandrasekaran and S. K. Nayak, "Study of Partial Discharges in Fresh and Oxidative Aged Mineral-Natural Ester Blended Oils," in *IEEE Transactions on Dielectrics and Electrical Insulation*, vol. 30, no. 5, pp. 2325-2333, Oct. 2023.

[9] H. Jin, P. Morshuis, A. R. Mor, J. J. Smit and T. Andritsch, "Partial discharge behavior of mineral oil based nanofluids", *IEEE Trans. Dielectr. Electr. Insul*., vol. 22, no. 5, pp. 2747-2753, Oct. 2015.

[10] M. Jaroszewski and K. Rakowiecki, "Partial discharge inception voltage in transformer natural ester liquid—Effect of the measurement method in the presence of moisture", *IEEE Trans. Dielectr. Electr. Insul.*, vol. 24, no. 4, pp. 2477-2482, Sep. 2017.

[11] R. Sangineni, S. K. Nayak and M. Becerra, "A non-intrusive and non-destructive technique for condition assessment of transformer liquid insulation", *IEEE Trans. Dielectr. Electr. Insul.*, vol. 29, no. 2, pp. 693-700, Apr. 2022.

[12] S. Chandrasekar, J. Chandramohan, G. C. Montanari and P. Uthirakumar, "Developing eco-friendly nanostructured oil: Partial discharge and breakdown voltage characterization of transformer corn oil," in *IEEE Transactions on Dielectrics and Electrical Insulation*, vol. 27, no. 5, pp. 1611-1618, Oct. 2020, doi: 10.1109/TDEI.2020.008992.

[13] S. N. Meitei, K. Borah and S. Chatterjee, "Partial Discharge Detection in an Oil-Filled Power Transformer Using Fiber Bragg Grating Sensors: A Review," in *IEEE Sensors Journal*, vol. 21, no. 9, pp. 10304-10316, 1 May1, 2021, doi: 10.1109/JSEN.2021.3059931.

[14] X. Li *et al.*, "Partial discharge characteristics of oil-paper insulation for on-board traction transformers under superposed inter-harmonic AC voltages," in *IEEE Transactions on Dielectrics and Electrical Insulation*, vol. 27, no. 1, pp. 240-248, Feb. 2020, doi: 10.1109/TDEI.2019.008404.

[15] J. Li, T. Jiang, C. Cheng and C. Wang, "Hilbert fractal antenna for UHF detection of partial discharges in transformers," in *IEEE Transactions on Dielectrics and Electrical Insulation*, vol. 20, no. 6, pp. 2017-2025, December 2013, doi: 10.1109/TDEI.2013.6678849.

[16] Q. Zhang, C. Li, S. Zheng, H. Yin, Y. Kan and J. Xiong, "Remote detecting and locating partial discharge in bushings by using wideband RF antenna array," in *IEEE Transactions on Dielectrics and Electrical Insulation*, vol. 23, no. 6, pp. 3575-3583, Dec. 2016, doi: 10.1109/TDEI.2016.005747.

[17] M. -K. Chen, J. -M. Chen and C. -Y. Cheng, "Partial discharge detection in 11.4 kV cast resin power transformer," in *IEEE Transactions on Dielectrics and Electrical Insulation*, vol. 23, no. 4, pp. 2223-2231, August 2016, doi: 10.1109/TDEI.2016.7556498.

[18] Ghaffarian Niasar, Mohamad. "Partial discharge signatures of defects in insulation systems consisting of oil and oil-impregnated paper." PhD diss., KTH Royal Institute of Technology, 2012.

[19] Zhao Liu, "Partial discharge and streamer characteristics of transformer liquids under AC stress." Thesis, The University of Manchester (United Kingdom), 2017.

[20] D. A. do Nascimento, S. S. Refaat, A. Darwish, Q. Khan, H. Abu-Rub, and Y. Iano, "Investigation of Void Size and Location on Partial Discharge Activity in High Voltage XLPE Cable Insulation," in *2019 Workshop on Communication Networks and Power Systems (WCNPS)*, Oct. 2019.

[21] Z. Wu, Q. Zhang, Z. Pei and H. Ni, "Correspondence between phase resolved partial discharge patterns and corona discharge modes," in *IEEE Transactions on Dielectrics and Electrical Insulation*, vol. 26, no. 3, pp. 898-903, June 2019, doi: 10.1109/TDEI.2018.007855.

[22] R. Zemouri and M. Lévesque, "Ensemble Deep-Learning Model for Phase-Resolved Partial Discharge Diagnosis in Hydrogenerators," in *IEEE Transactions on Dielectrics and Electrical Insulation*, vol. 30, no. 5, pp. 2394-2401, Oct. 2023, doi: 10.1109/TDEI.2023.3267060.

[23] M. A. Saleh, S. S. Refaat, M. Olesz and H. Abu-Rub, "Inception and Propagation of Electrical Trees in the Presence of Space Charge in HVAC Extruded Cables," in *IEEE Transactions on Dielectrics and Electrical Insulation*, vol. 28, no. 5, pp. 1775-1784, October 2021.

[24] M. A. Saleh and S. S. Refaat, "The Impact of Water Trees and Cavities on the Electric Field Distribution in XLPE Power Cables," *2019 2nd International Conference on Smart Grid and Renewable Energy (SGRE)*, Doha, Qatar, 2019, pp. 1-8.

[25] B. Ge and D. C. Ludois, "Dielectric liquids for enhanced field force in macro scale direct drive electrostatic actuators and rotating machinery," in *IEEE Transactions on Dielectrics and Electrical Insulation,* vol. 23, no. 4, pp. 1924-1934, August 2016, doi: 10.1109/TDEI.2016.7556463.

[26] F. T. Ulaby and U. Ravaioli, Fundamentals of Applied Electromagnetics. *Prentice Hall*, 2015.

[27] G. Grimmett and D. Stirzaker, *Probability and Random Processes*. Oxford University Press, 2001.

[28] "Derived Value." https://doc.comsol.com/5.5/doc/com.comsol.help.comsol/comsol_ref_solver.27.201.html (accessed Oct. 19, 2023).

[29] M. Florkowski, B. Florkowska, J. Furgał and P. Zydron, "Impact of high voltage harmonics on interpretation of partial discharge patterns," in *IEEE Transactions on Dielectrics and Electrical Insulation*, vol. 20, no. 6, pp. 2009-2016, December 2013, doi: 10.1109/TDEI.2013.6678848.

[30] Q. Khan, S. S. Refaat, H. Abu-Rub, H. A. Toliyat, M. Olesz and A. Darwish, "Characterization of Defects Inside the Cable Dielectric With Partial Discharge Modeling," in *IEEE Transactions on Instrumentation and Measurement*, vol. 70, pp. 1-11, 2021, Art no. 3502911, doi: 10.1109/TIM.2020.3027925.

[31] E. M. Stein and R. Shakarchi, Fourier Analysis: An Introduction. Princeton University Press, 2003.

[32] S. M. Kameli, S. S. Refaat, H. Abu-Rub, A. Darwish, A. Ghrayeb and M. Olesz, "Ultrawideband Vivaldi Antenna With an Integrated Noise-Rejecting Parasitic Notch Filter for Online Partial Discharge Detection," in *IEEE Transactions on Instrumentation and Measurement*, vol. 73, pp. 1-10, 2024, Art no. 8001610, doi: 10.1109/TIM.2024.3353284.

Sayed Mohammad Kameli (Student Member, IEEE) holds a Bachelor of Science in Electrical Engineering since 2022 from Texas A&M University at Qatar, Doha, Qatar.

His work experience includes working as a Student Research Assistant, a Program Aide, and a Research Assistant at Texas A&M University at Qatar, Doha, Qatar. His research interests involve antennas and partial discharge detection in power transformers and gas-insulated switchgear. Mr. Kameli is a student member of the Institution of Engineering and Technology (IET).

Abdelaziz Abuelrub. Abdelaziz Abuelrub is an undergraduate Electrical and Computer Engineering student at Texas A&M University, Doha, Qatar.

His work experience includes working as a Student Research Assistant at Texas A&M University at Qatar. His research interests involve Finite Element Analysis, deep learning, and partial discharge detection in different high voltage power cables and transformers.

Mr. Abuelrub is a student member of the IEEE.

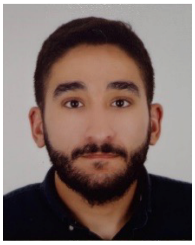

Mohammad AlShaikh Saleh (Student Member, IEEE) received his B.Sc. degree in Electrical Engineering in 2020 from the University of Applied Sciences Upper Austria, Wels, Austria. He then acquired his M.Sc. degree in Power Engineering in 2022 from the Technical University of Munich, Munich, Germany. Currently, he is pursuing his Ph.D. at the Department of Electrical and Computer Engineering at Texas A&M University, College Station, TX, USA, where his research focuses on estimating the remaining useful lifetime of rotating machines, power cables, power transformers, gas-insulated switchgears, and Li-ion batteries using Machine Learning and Finite Element Analysis (FEA).

Shady S. Refaat (Senior Member, IEEE) received the B.A.Sc, M.A.Sc., and Ph.D. degrees in Electrical Engineering in 2002, 2007, and 2013, respectively, all from Cairo University, Giza, Egypt. He has worked in the industry for more than 12 years as Engineering Team Leader, Senior Electrical Engineer, and Electrical Design Engineer on various electrical engineering projects. He has worked as an associate research scientist in the Department of Electrical and Computer Engineering, Texas A&M University at Qatar for more than 11 years. Currently, he is a senior lecturer at the University of Hertfordshire. He is a senior member of the Institute of Electrical and Electronics Engineers (IEEE), a member of The Institution of Engineering and Technology (IET), a member of the Smart Grid Center – Extension in Qatar (SGC-Q). He has published more than 195 journal and conference articles, one patent, and one book. His principal work area focuses on electrical machines, power systems, smart grid, Big Data, energy management systems, reliability of power grids and electric machinery, fault detection, and condition monitoring and development of fault-tolerant systems. Also, he has participated and leads several scientific projects over the last nine years. He has successfully realized many potential research projects.

Ali Ghrayeb (Fellow, IEEE) received the Ph.D. degree in electrical engineering (EE) from The University of Arizona, Tucson, AZ, USA, in 2000.

He is currently a Professor in Electrical and Computer Engineering with College of Science and Engineering, Hamad Bin Khalifa University, Qatar Foundation, Doha, Qatar. His research interests include massive MIMO, wireless communications, physical layer security, and visible light communications.

Haitham Abu-Rub (Fellow, IEEE) received the M.Sc. degree in electrical engineering from Gdynia Maritime Academy, Gdynia, Poland, in 1990, the Ph.D. degree in electrical engineering from the Technical University of Gdansk, Gdansk, Poland, in 1995, and the Ph.D. degree in humanities from Gdansk University, Gdansk, Poland, in 2004.

He is a Professor with Hamad bin Khalifa University, Ar-Rayyan, Qatar. He has research and teaching experiences at many universities in many countries including Qatar, Poland, Palestine, USA, and Germany. He has served for five years as the chair of Electrical and Computer Engineering Program with Texas A&M University at Qatar and for ten years as the Managing Director with the Smart Grid Center at the same university. He has coauthored more than 600 journal and conference papers, 6 books, and 6 book chapters. His main research interests include energy conversion systems, smart grids, renewable energy systems, electric drives, and power electronic converters.

Dr. Abu-Rub was the recipient of many prestigious national and international awards and recognitions, such as the American Fulbright Scholarship and the German Alexander von Humboldt Fellowship. He is the Co-Editor-in-Chief for IEEE TRANSACTIONS ON INDUSTRIAL ELECTRONICS.

Marek Olesz received the M.Sc., Ph.D., and D.Sc. degrees in electrical engineering from Faculty of Electrical and Control Engineering, Gdansk University of Technology, Poland, in 1990, 1998, and 2017, respectively. He is currently an Associate Professor with the Department of Electrical Power Engineering, Gdansk University of Technology. For many years, he has participated in intense research for respected, important manufactures and companies, both Polish (Energa, PTPIREE, PERN, Apator, Miflex, SAG Elbud, and Group Base) and foreign ones (ABB and Aseco). This cooperation considers technical aspects of high voltage and electrical apparatus, electrical safety, lightning and overvoltage protection, product conformity, and power quality. His research interests include diagnostics and simulation of ZnO surge arresters, power cables, and uninterruptible power supplies. He received the Rector's Award, medals, and diplomas both for scientific and educational achievements.